Res Chem Intermed
DOI 10.1007/s11164-016-2722-5

Spectroscopic, thermal, non-isothermal decomposition kinetics and quantum chemical computational studies of Ni(II)- and Cu(II)-Schiff base complexes

Brajendra S. Kusmariya[1] · Anjali Tiwari[1] · Gowhar Ahmad Naikoo[2] · A. P. Mishra[1]

Received: 1 April 2016 / Accepted: 31 August 2016

Abstract Herein we report spectroscopic, thermal, non-isothermal decomposition kinetics and theoretical studies of two mononuclear Ni(II)- and Cu(II)-complex of general formula $[M(L)(H_2O)]\cdot xH_2O$; {M = Ni(II) & Cu(II)} derived from tridentate 2,4-dichloro-6-{[(5-chloro-2-sulfanylphenyl)imino]methyl}phenol ligand (H_2L). These compounds were synthesized and characterized by various physicochemical and spectral techniques. Thermal decomposition of complexes was studied in four steps at different temperature regions to understand the degradation pattern of complexes under nitrogen atmosphere up to 1073 K at the 10 K min^{-1} heating rate. The non-isothermal kinetic parameters viz. activation energy (E^*), pre-exponential factor (Z), entropy of activation (ΔS^*), enthalpy of activation (ΔH^*) and free energy of activation (ΔG^*) of degradation process were calculated using Coats–Redfern (C–R), Piloyan–Novikova (P–N) and Horowitz–Metzger (H–M) methods assuming first order degradation and proposing a random nucleation mechanism of thermal decomposition. Quantum chemical computational investigations were carried out at the B3LYP level using 6-31G basis set. The calculated harmonic vibrations were compatible with the observed FTIR and Raman

Electronic supplementary material The online version of this article (doi:10.1007/s11164-016-2722-5) contains supplementary material, which is available to authorized users.

✉ A. P. Mishra
apmishrasagar@gmail.com

Brajendra S. Kusmariya
kusmariya@gmail.com

Anjali Tiwari
Anjalitiwari0001@gmail.com

Gowhar Ahmad Naikoo
gowhar@du.edu.om

[1] Department of Chemistry, Dr. H. S. Gour Central University, Sagar 470003, India

[2] Department of Mathematics and Sciences, College of Arts and Applied Sciences, Dhofar University, Salalah, Sultanate of Oman

Published online: 17 September 2016

frequencies. The thermodynamic properties ($C_{p,m}°$; $S_m°$ and $H_m°$) with varying temperatures up to 500 K and non-linear optical properties were also evaluated at the same level of theory.

Graphical Abstract

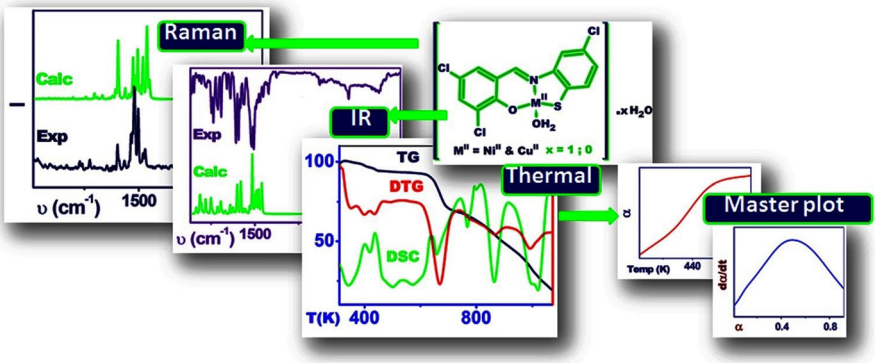

Keywords Schiff base-metal complexes · Thermal studies · Non-isothermal kinetic parameters · Raman frequencies · DFT

Introduction

In the modern age, the introduction of sophisticated physicochemical techniques of higher accuracy and potential have greatly enriched our understanding to the nature of the metal–ligand bond, the structural features of metal complexes, their stability and other properties. The well-established thermogravimetry and differential scanning calorimetry techniques have been consistently used in studying the thermal behavior and properties of various types of materials for many years [1, 2]. In association with other characterization techniques like FTIR, PXRD, Mass; etc., thermal studies provide valuable structural information. Kinetic parameters of non-isothermal degradation steps of metal complexes obtained by thermoanalytical methods may be evaluated by several methods [3, 4].

The knowledge of the mechanism of non-isothermal degradation allows the postulation of kinetic equations or vice versa [5]. There are different methods to study the kinetics of non-isothermal processes including statistical methods [6, 7], methods for different reaction models, Coats–Redfern (C–R) [8], Piloyan–Novikova (P–N) [9], Horowitz–Metzger (H–M) [10], and iso-conversional model free methods [11].

In the last three decades, DFT has become the most popular and useful computational approach to predict fairly accurate structural information for the compounds [12, 13]. Many workers reported comparable studies of calculated harmonic vibrational frequencies with experimental IR and Raman frequencies of Schiff base complexes. They also described thermodynamic functions obtained

from the theoretical harmonic frequencies and their correlations with temperatures [14, 15]. Earlier we reported synthesis and structural characterization supported by DFT of 2,4-dichloro-6-{[(5-chloro-2-sulfanylphenyl)imino]methyl}phenol ligand and its mononuclear 3*d*-complexes [16, 17]. Here, we extend our work to solid state reaction kinetics and additional theoretical works for the Ni(II)- and Cu(II)-complex.

In the present paper; the solid state reaction model, non-isothermal degradation kinetics and mechanisms using different forms of kinetic models for the Ni(II)- and Cu(II)-complex of 2,4-dichloro-6-{[(5-chloro-2-sulfanylphenyl)imino]methyl}phenol ligand are reported. The present work also reports comparative studies of experimental FTIR and Raman frequencies with calculated vibrational frequencies. In addition, thermodynamic functions ($C_{p,m}°$; $S_m°$ and $H_m°$) with varying temperatures up to 500 K and non-linear optical properties are also computed at the B3LYP level using the 6-31G basis set.

Experimental

Reagents and instruments

All the reagents were obtained commercially (3,5-dichloro-2-hydroxybenzaldehyde, Mol.Wt. 192.01 g mol^{-1}; Nickel chloride hexahydrate $NiCl_2{\cdot}6H_2O$, Mol.Wt. 237.69 g mol^{-1}; Copper chloride dihydrate $CuCl_2{\cdot}2H_2O$, Mol.Wt. 170.48 g mol^{-1} from Aldrich, India and 2-amino-4-chlorobenzenethiol, Mol.Wt. 159.64 g mol^{-1}; from TCI Fine Chemicals) with analytical grade and used as such. Commercial organic solvents were distilled and then used for the synthesis. Molar conductance of the complexes was recorded in DMF (1×10^{-3} M) at room temperature using a Systronic model-304 digital conductivity meter. The FTIR spectra were recorded as KBr discs in the range of 4000–400 cm^{-1} on a Shimadzu FT IR-8400 S instrument. Thermal data were collected on a NETZSCH STA instrument under nitrogen atmosphere (nitrogen and air in 6:4 ratios) at the heating rate of 10 K min^{-1} from room temperature to 1073 K. The Raman spectra of the solid samples were measured in the region 3200–50 cm^{-1} with a spectral resolution of 1.0 cm^{-1} in the backscattering configuration on a RENISHAW inVia Raman microscope with a He–Ne laser source (635 nm).

Synthesis of the metal complexes $[M(L)(H_2O)]{\cdot}xH_2O$ {M = Ni(II) and Cu(II)}

Synthesis of ligand and its metal complexes were discussed in detail earlier [16, 17]. Methanolic solutions of Metal(II) salts (1 mmol), were added dropwise to the methanolic solution of Schiff base (1 mmol) in slightly alkaline medium by adding a few drops of aq. KOH solution (5 % w/v). The reaction mixture was stirred and refluxed for 1 h until precipitation was observed; furthermore, the colored precipitates were filtered, washed with methanol and diethyl ether, and dried in vacuum over fused $CaCl_2$.

[Ni(L)(H_2O)]·H_2O

Mol. Formula: $C_{13}H_8Cl_3NiNO_2S$; Mol. Wt.: 407.3; Yield 58 %; Color: yellowish brown.
Anal. Calc.: C-38.33, H-1.98, N-3.44; Found: C-38.67, H-1.99, N-3.12;
Molar conductance (DMF) λ_m(cm^2 Ω^{-1} mol^{-1}): 20.56

[Cu(L) (H_2O)*]*

Mol. Formula: $C_{13}H_8Cl_3CuNO_2S$; Mol. Wt.: 412.2; Yield 57 %; Color: green.
Anal. Calc.: C-37.88, H-1.96, N-3.40; Found: C-38.04, H-1.98, N-3.33;
Molar conductance (DMF) λ_m(cm^2 Ω^{-1} mol^{-1}): 24.14

Theoretical calculations

The quantum chemical computation of Ni(II)- and Cu(II)-complex were performed at the DFT level employing Becke's three parameter hybrid exchange functional and the Lee–Yang–Parr correlation functional (B3LYP) [18, 19] using the 6-31G and LANL2DZ basis set with the help of Gaussian 03 W and Gauss view 3.0 software [20]. Furthermore, visualization of optimized structures was performed by means of the Chemcraft 1.7 program package [21]. The gas-phase vibrational frequencies, non-linear optical properties and thermodynamic properties were computed based on optimized molecular geometry by using B3LYP with the 6-31G basis set.

Results and discussion

The physical and analytical data of synthesized compounds suggest the ligand to metal ratio was 1:1 (M:L) with general composition of $[M(L)(H_2O)]\cdot xH_2O$ {M = Ni(II) & Cu(II); $x = 0$ & 1}. This was in agreement with elemental analyses data. Both complexes were colored, stable at room temperature, and soluble in DMF and DMSO. The molar conductance measurements of the complexes were recorded in DMF (1×10^{-3} M). The low conductance values of the complexes indicated their non-electrolytic nature [17]. The synthetic scheme of the ligand and its complexes used in the present work are represented in Fig. 1.

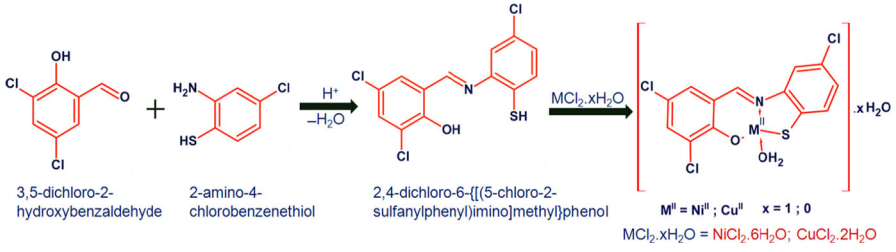

Fig. 1 Synthetic scheme of ligand and its Ni(II)- and Cu(II)-complex

Thermal studies

The thermal behavior of metal complexes shows that the hydrated complexes lose molecules of hydration first; followed by decomposition of ligand molecules in the subsequent steps [22]. To understand the thermal behavior of the Ni(II)- and Cu(II)-complex; the TG graphs of complexes were analyzed (2) which showed a multistep decomposition pattern. It was also noted that any stable intermediates were not formed during the decomposition process.

As evident from TG, DSC, and DTG curves of $[Ni(L)(H_2O)]\cdot H_2O$; the complex shows four steps in the decomposition process. Elimination of one lattice water molecule was observed to raise the temperature up to 390 K (Step-I dehydration, wt%, obs./calcd. 4.52/4.23). Another weight loss corresponds to one coordinated water molecule observed in the range of 395–465 K (Step-II dehydration, wt%, obs./calcd. 4.86/4.23). In the third step of decomposition in the range of 580–710 K, a loss in weight was observed corresponding to the loss of a partially decomposed ligand part from the complex (Step-III oxidative degradation, wt%, obs./calcd. 24.82/26.04). Above this temperature, a weight loss occurred up to the final temperature (Step-IV oxidative degradation, wt%, obs./calcd. 46.84/46.28). This indicates the elimination of the remaining thermally degradable part of the complex. By dehydration, oxidative degradation and rearrangements, the degradable part of the complex converted into gaseous product viz. H_2O, CO_2, CO, NO_x, SO_x etc., and the ultimate pyrolysis product has been projected to be nickel(II) oxide (residue, wt%, obs./calcd. 18.96/18.03) (Fig. 2).

In the TG graph of $[Cu(L)(H_2O)]$; decomposition of the complex was observed at three steps in the range of 460–550, 560–750 and 770–1072 K, respectively. The complex did not show any loss in weight up to 460 K, indicating the absence of lattice water molecules. Elimination of one coordinated water molecule was observed on raising the temperature up to 550 K (step-I dehydration, @wt%, obs./calcd. 4.92/4.36). After this temperature, a loss in weight was observed in general up to 750 K corresponding to the loss of a partially decomposed ligand part from the complex (step-II oxidative degradation, wt%, obs./calcd. 24.42/25.80). Above this temperature, a weight loss occurred up to the final temperature (step-III oxidative degradation, wt%, obs./calcd. 49.47/47.06). This indicates the elimination of the remaining thermally degradable part of the complex. The ultimate pyrolysis product was obtained as copper (II) oxide (residue, wt%, obs./calcd. 21.19/19.78). The relatively higher percentage of final pyrolysis product may be due to the formation of some other species, e.g., metal carbides or metal oxides accompanied by carbon deposits [17].

Non-isothermal degradation of $[Ni(L)(H_2O)]\cdot H_2O$ $\{L = C_{13}H_8Cl_3NOS\}$:

$[Ni(C_{13}H_8Cl_3NOS)(H_2O)]\cdot H_2O \rightarrow [Ni(C_{13}H_8Cl_3NOS)] + H_2O$

(Step-I, II; Dehydration)

$[Ni(C_{13}H_8Cl_3NOS)] \rightarrow NiO +$ non-degradable residue $+ CO_2 + CO + NO_x + SO_x + Cl_2$

(Step-III, IV; Oxidative degradation)

Non-isothermal degradation of $[Cu(C_{13}H_8Cl_3NOS)(H_2O)]$ $\{L = C_{13}H_8Cl_3NOS\}$:

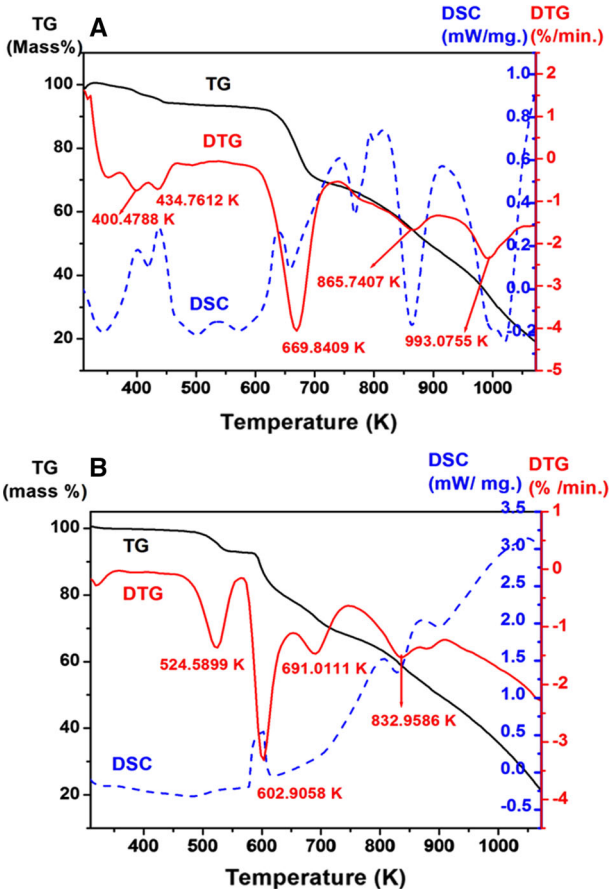

Fig. 2 Combined TG, DTG, and DSC graphs of (A) $[Ni(L)(H_2O)]\cdot H_2O$ (B) $[Cu(L)(H_2O)]$ complex in the range of 300–1073 K and 10 K min^{-1} heating rate under nitrogen atmosphere

$$[Cu(C_{13}H_8Cl_3NOS)(H_2O)] \rightarrow [Cu(C_{13}H_8Cl_3NOS)] + H_2O$$
(Step-I; Dehydration)
$$[Cu(C_{13}H_8Cl_3NOS)] \rightarrow CuO + \text{non-degradable residue} + CO_2 + CO + NO_x + SO_x + Cl_2$$
(Step-II, III; Oxidative degradation)

Kinetic study

To determine the correct model for kinetics; non-isothermal $d\alpha/dT$ and α temperature plots for both complexes were drawn and are represented in Figs. 3 and 4 and supporting information (Figs. S1–S6). The shape of these plots was shown to be a close resemblance with the first order model. The first-order model, also

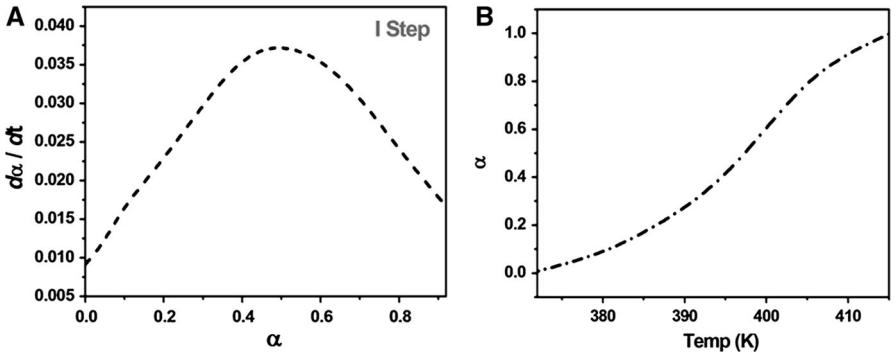

Fig. 3 Master plot for I step of thermal degradation of $[Ni(L)(H_2O)]\cdot H_2O$ complex for determining a solid state reaction model; **a** $d\alpha/dT$ versus α and **b** α versus *temperature*; data simulated with a heating rate of 10 K min^{-1}

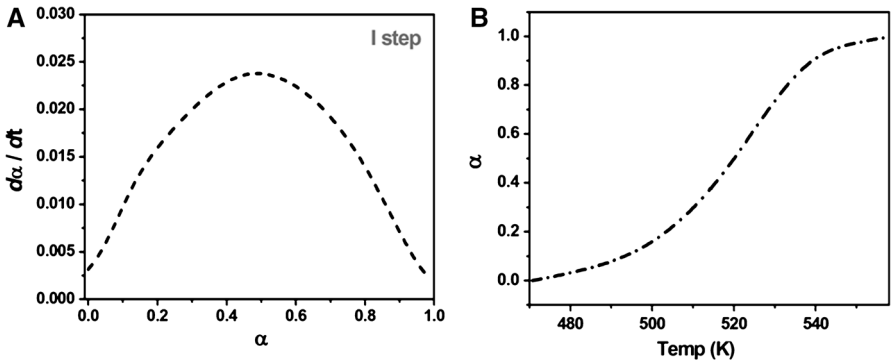

Fig. 4 Master plot for I step of thermal degradation of $[Cu(L)(H_2O)]$ complex for determining a solid state reaction model; **a** $d\alpha/dT$ versus α and **b** α versus *temperature*; data simulated with a heating rate of 10 K min^{-1}

known as the Mampel model, is a special case of the Avrami–Erofeyev (A) models where $n = 1$ [23].

On the basis of thermal decomposition; the non-isothermal kinetic parameters viz. activation energy (E^*), pre-exponential factor (Z), entropy of activation (ΔS^*), enthalpy of activation (ΔH^*) and free energy of activation (ΔG^*) of each thermal degradation stage were evaluated using Coats–Redfern (C–R) [8], Piloyan–Novikova (P–N) [9] and Horowitz–Metzger (H–M) [10] methods.

The thermal degradation was assumed to be first order ($n = 1$) in all the degradation steps, and the calculated kinetic parameters were summarized in Tables 1 and 2. The best results had been obtained by using the C–R method in all three methods for calculating nonisothermal kinetic parameters of both complexes. In the C–R method, the $\log[g(\alpha)/T^2]$ was plotted against 1/T as shown in Figs. 5 and 6. The data obtained were recorded in Tables 1 and 2. The activation energy of the compound directly related to its thermal stability, e.g., higher for the E^* then the higher the stability of complexes [24]. The activation energy E^* of

Table 1 Non-isothermal kinetic parameters E^*, Z, ΔS^*, ΔH^* and ΔG^* of Ni(II)-complex calculated by the C–R, P–N and the H–M method

Method	Decomposition step (DTG peak in K)	r^2	Nonisothermal kinetic parameter				
			E^* (kJ mol^{-1})	Z (s^{-1})	ΔS^* (kJ mol^{-1} K^{-1})	ΔH^* (kJ mol^{-1})	ΔG^* (kJ mol^{-1})
C–R	I (400.48)	0.994	0.139487	2.55019E+13	0.009293	−3.19009	−6.91188
	II (434.76)	0.973	0.166523	8.98488E+14	0.03823	−3.44808	−20.0689
	III (669.84)	0.985	0.175732	259,352,680.5	−0.09058	−5.39332	55.28056
	IV (865.74)	0.994	0.246041	3,304,043,947	−0.07155	−6.95173	54.994
P–N	I (400.48)	0.954	0.104697	328,073,531.4	−0.08435	−3.22488	30.55457
	II (434.76)	0.89	0.088153	139,084.2659	−0.14961	−3.52645	61.51735
	III (669.84)	0.922	0.118578	3846.305426	−0.18304	−5.45048	117.156
	IV (865.74)	0.961	0.162732	13,567.83386	−0.17469	−7.03504	144.2004
H–M	I (400.48)	0.991	0.150677	2.55019E+13	0.009293	−3.1789	−6.90069
	II (434.76)	0.971	0.166578	8.98488E+14	0.03823	−3.44803	−20.0689
	III (669.84)	0.98	0.186519	259,352,680.5	−0.09058	−5.38254	55.29135
	IV (865.74)	0.993	0.255487	3,304,043,947	−0.07155	−6.94228	55.00345

Table 2 Nonisothermal kinetic parameters E^*, Z, ΔS^*, ΔH^* and ΔG^* of the Cu(II)-complex calculated by the C–R, P–N and the H–M method

Method	Decomposition step (DTG peak in K)	r^2	Nonisothermal kinetic parameter				
			E^* (kJ mol^{-1})	Z (s^{-1})	ΔS^* (kJ mol^{-1} K^{-1})	ΔH^* (kJ mol^{-1})	ΔG^* (kJ mol^{-1})
C–R	I (524.59)	0.996	0.139487	25.20238	−0.22282	−4.22195	112.6648
	II (602.91)	0.971	0.574414	1.03E+45	0.611031	−4.43814	−372.832
	III (691.01)	0.986	0.160262	5,222,376	−0.12331	−5.5848	79.62535
	IV (832.959)	0.968	0.323778	8.17E+14	0.032034	−6.60144	−33.2843
P–N	I (524.59)	0.947	0.104352	87,809.03	−0.15499	−4.25709	77.05139
	II (602.91)	0.96	0.533248	1.99E+41	0.539951	−4.47931	−330.019
	III (691.01)	0.923	0.086124	21.63526	−0.22638	−5.65894	150.7692
	IV (832.959)	0.893	0.229957	5.65E+08	−0.08592	−6.69526	64.87592
H–M	I (524.59)	0.992	0.160158	25.20238	−0.22282	−4.20128	112.6854
	II (602.91)	0.969	0.601398	1.03E+45	0.611031	−4.41116	−372.805
	III (691.01)	0.984	0.166736	5,222,376	−0.12331	−5.57833	79.63182
	IV (832.959)	0.964	0.3288	8.17E+14	0.032034	−6.59642	-33.2793

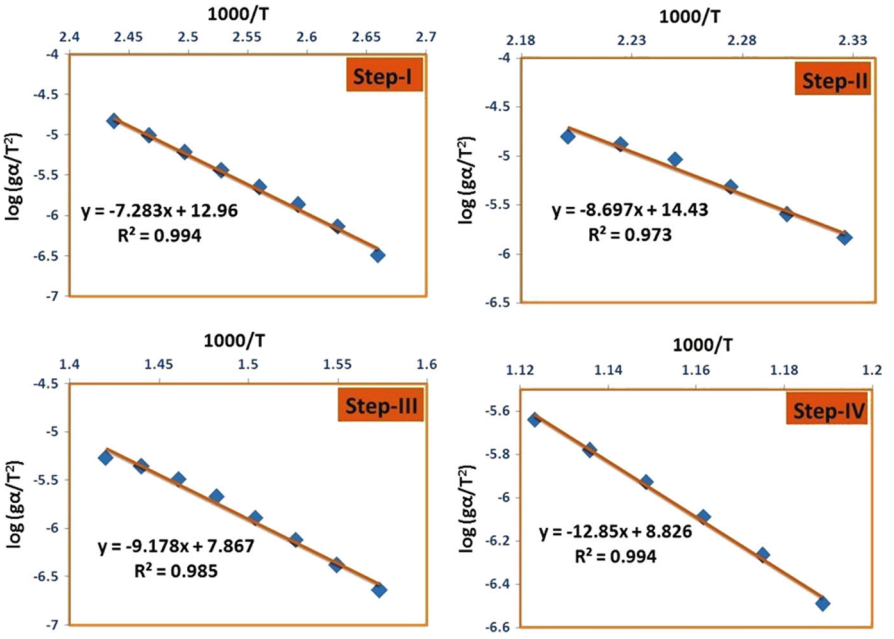

Fig. 5 Coats–Redfern (C–R) plot of the different degradation steps for the $[Ni(L)(H_2O)]\cdot H_2O$ complex

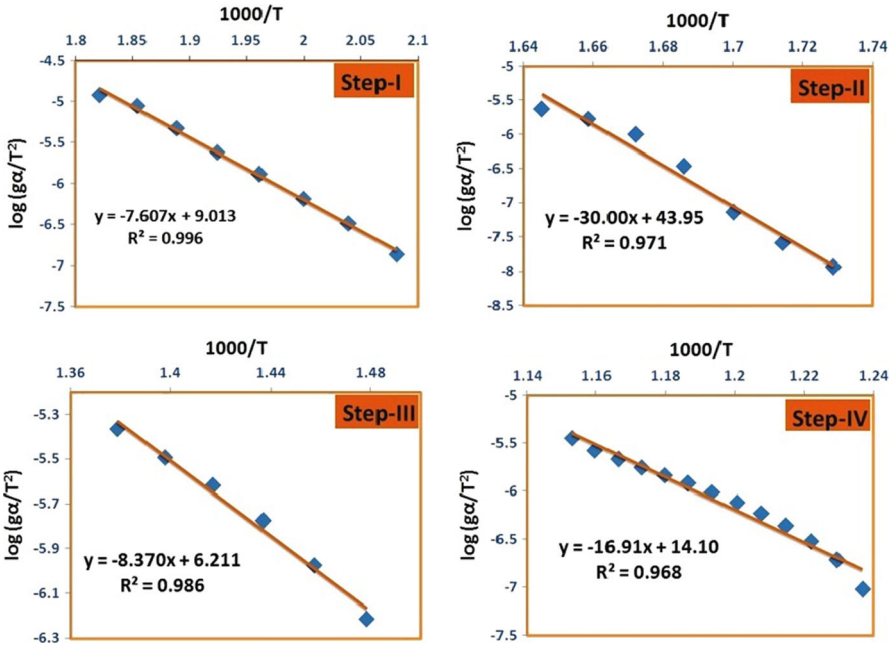

Fig. 6 Coats–Redfern (C–R) plot of different degradation steps for the $[Cu(L)(H_2O)]$ complex

$[Ni(L)(H_2O)]\cdot H_2O$ and $[Cu(L)(H_2O)]$ complexes in different stages were found to be 0.0139–0.2460 and 0.139–0.5744 kJ mol^{-1}, respectively, calculated by the C–R method. The relatively higher E^* of the Cu(II)-complex makes it more stable compared to the Ni(II)-complex. The activation energy E^* was found to be highest for the second step in the copper complex, which means that dehydrated complex was more stable and facing less steric strain at this stage. The entropy of activation ΔS^* were found in the range of −0.0906 to 0.0382 kJ mol^{-1} K^{-1} for the Ni(II)-complex and −0.2228 to 0.6110 kJ mol^{-1} K^{-1} for the Cu(II)-complex. The negative values of ΔS^* indicated that the activated complexes were a more ordered structure than the reactants or intermediates and degraded at a slower rate than normal [25].

Mechanistic aspects

The mechanism of thermal degradation is based on the assumption that the forms of $g(\alpha)$ depend on the reaction mechanism. So twenty-three different forms of $g(\alpha)$ were used to recognize the mechanism of the selected thermal degradation step [26, 27]. The regression coefficient (r^2) and activation energy (E^*) for all those twenty-three forms of $g(\alpha)$ were calculated from selected steps and the best fit had been chosen, which gave maximum r^2 value. The calculated values of r^2 and E^* for all twenty-three forms of $g(\alpha)$ are given in Table 3. The maximum value of r^2 had been obtained for S5 $[g(\alpha) = -\ln(1 - \alpha)]$ from all degradation steps of $[Ni(L)(H_2O)]\cdot H_2O$ and $[Cu(L)(H_2O)]$ complexes, which represent the random nucleation mechanism of thermal decomposition with one nucleus for each particle.

Theoretical calculations

The molecular geometries of synthesized compounds in gas phase were fully optimized with respect to the energy using the 6-31G and LANL2DZ basis set at the B3LYP level and the main optimized geometrical parameters, e.g., selected bond lengths and bond angles; HOMO–LUMO, spin densities, Mulliken charge distribution, MEP; etc., were described earlier [16, 17].

The FTIR and Raman frequencies

There are some characteristic peaks, in the spectrum of ligand, which are of good help for determining the coordination sites. The position and intensities of these peaks were expected to change on chelation. The FT-IR spectrum of the ligand exhibited some characteristic bands at 1614.5 cm^{-1} υ(–HC=N–), 1271.1 cm^{-1} υ(C–O), 1068.6 cm^{-1} υ(C–S) 2815–3025 cm^{-1} υ(O–H) and 2360.8 cm^{-1} υ(S–H). The υ(O–H) stretching vibration observed at a comparatively lower region in the range of 2815–3025 cm^{-1} suggests that the parent compound shows the intra-molecular H bond of O–H–N type [16].

An insight on the FTIR spectra of the investigated complexes shows that the ligand behaves as a binegative tridentate in the Ni(II)- and Cu(II)-complex coordinating through a deprotonated thiolic sulfur atom (C–S–), a deprotonated enolic oxygen atom (C–O–), and an azomethine nitrogen atom (C=N). This

Table 3 Regression coefficient (r^2) and activation energy (E^*) calculation using the twenty-three forms of $g(\alpha)$ functions for the $[Ni(L)(H_2O)]\cdot H_2O$ (III-step) and the $[Cu(L)(H_2O)]$ (II-step)

Mechanism	Integral form $g(\alpha)$	$[Ni(L)(H_2O)]\cdot H_2O$		$[Cu(L)(H_2O)]$	
		III-step (DTG peak: 669.84 K)		II-step (DTG peak: 602.91 K)	
		r^2	E	r^2	E
S1	$[-\ln(1-\alpha)]^{1/4}$	0.9581	0.046018241	0.8232	0.074293
S2	$[-\ln(1-\alpha)]^{1/3}$	0.9641	0.065046671	0.815	0.090376
S3	$[-\ln(1-\alpha)]^{1/2}$	0.969	0.103101616	0.826	0.140617
S4	$[-\ln(1-\alpha)]^{2/3}$	0.9712	0.14115656	0.8312	0.190855
S5	$[-\ln(1-\alpha)]$	0.985	0.175732	0.971	0.574414
S6	α	0.8894	0.181775307	0.7415	0.224979
S7	$2[1-(1-\alpha)^{1/2}]$	0.9355	0.181775307	0.7893	0.255231
S8	$3[1-(1-\alpha)^{1/3}]$	0.9494	0.141273358	0.8052	0.266586
S9	α^2	0.8982	0.374613833	0.7501	0.460068
S10	$(1-\alpha)\ln(1-\alpha)+\alpha$	0.9235	0.393914152	0.7783	0.497079
S11	$(1-2\alpha/3)-(1-\alpha)^{2/3}$	0.9343	0.402032541	0.7897	0.512301
S12	$[1-(1-\alpha)^{1/3}]^{-2}$	0.9529	0.41865226	0.8111	0.543281
S13	$[(1+\alpha)^{1/3}-1]^2$	0.8828	0.355964517	0.7296	0.425603
S14	$[(1/(1-\alpha)^{1/3}-1]^2$	0.99	0.476017097	0.8687	0.64771
S15	$\alpha^{1/4}$	0.8061	0.03714737	0.6815	0.04867
S16	$\alpha^{1/3}$	0.8412	0.053215652	0.7033	0.06826
S17	$\alpha^{1/2}$	0.8683	0.085356044	0.9008	0.134354
S18	$\alpha^{2/3}$	0.8795	0.117496437	0.7326	0.146623
S19	$\alpha^{3/2}$	0.8954	0.278188826	0.7473	0.342523
S20	$\alpha^{3/4}$	0.8823	0.133566633	0.7356	0.166213
S21	$[(1-\alpha)^{-1}-1]$	0.9992	0.267830222	0.9137	0.381641
S22	$[1-(1-\alpha)^{1/2}]$	0.9355	0.197694241	0.7893	0.255231
S23	$[1-(1-\alpha)^{1/3}]$	0.9494	0.203802179	0.8052	0.266586

r^2 Regression coefficient; E kJ mol^{-1}

behavior is supported by: (1) The disappearance of the υ(S–H) band and the shifts of υ(C–S) to higher wavenumber (1068.6 cm^{-1}–1078.2 cm^{-1} for Ni(II)-complex and 1082.1 cm^{-1} for Cu(II)-complex). (2) Shift of υ(C–O) to lower wavenumber (1272.1–1251.8 cm^{-1} for Ni(II)-complex and 1253.8 cm^{-1} for Cu(II)-complex). (3) Shift of υ(–HC=N–) to lower wavenumber (1614.5–1583.6 cm^{-1} for Ni(II)-complex and 1587.5 cm^{-1} for Cu(II)-complex). (4) Appearance of two new bands of weak intensity corresponding to υ(M–N) and υ(M–O) vibration in the range of 445–459 and 522–547 cm^{-1} respectively. The band corresponding to the (M–S) stretching vibration appears at below 400 cm^{-1}, and; hence, could not be recorded in the present studies. Two new additional bands appeared around 850–862 and 580–590 cm^{-1} regions due to $\delta_r(H_2O)$ rocking and $\delta_w(H_2O)$ wagging vibrations,

respectively, due to coordinated water molecules. The appearance of broad bands around 3450–3700 cm^{-1} indicates the presence of water molecules. This is also confirmed by the thermal studies [17].

The harmonic vibrational frequencies were calculated at the B3LYP level using the 6-31G basis set for both complexes. The experimental FT-IR and Raman frequencies had been compared with the calculated vibration frequencies and listed in Tables S1 and S2. The calculated and observed FTIR and Raman spectra of both complexes are given in Figs. 7 and 8 and supporting information (Figs. S7 and S8). The characteristic υ(–HC=N–) stretching vibration for the Ni(II)-complex was computed at 1619.8 $cm^{-1,}$ which was observed at 1583.6 cm^{-1} in the IR region; 1587.0 cm^{-1} in the Raman region. Similarly, in the Cu(II)-complex it was computed at 1616.0 cm^{-1} and observed at 1587.5 cm^{-1} in the IR region; 1584.0 cm^{-1} in the Raman region. The stretching vibrations of water molecules present in complexes were computed theoretically at 3858.2 and 3660.6 cm^{-1} for the Ni(II)-complex and 3812.6 and 3604.9 cm^{-1} for the Cu(II)-complex. These vibrations were not seen in computed Raman spectra. In the Ni(II)-complex some other functional group frequencies observed in the FTIR region were 1217.12, 1078.2, 1554.67, 547.24, and 459.20 cm^{-1} assigned to (C–N), (C–S), (H_2O), (M–O), and (M–N) vibrations. The theoretical frequencies corresponding to those functional groups were computed at 1216.59, 1091.48, 1589.87, 686.18, and 531.54 $cm,^{-1}$ respectively. Similar results were seen in the Cu(II)-complex.

In Raman spectra of both complexes, a limited number of peaks compared to IR were observed and most intense peaks were mainly due to the (–C=C–)/ring and C–H Bending vibrations. This was also satisfied with the low intensity of calculated Raman frequencies for other functional groups.

The theoretical group frequencies show little deviations from experimental values and appear at comparatively higher wave numbers, which may be due to the negligence of anharmonicity in the B3LYP method. However, the theoretical–experimental agreement was found to be satisfactory.

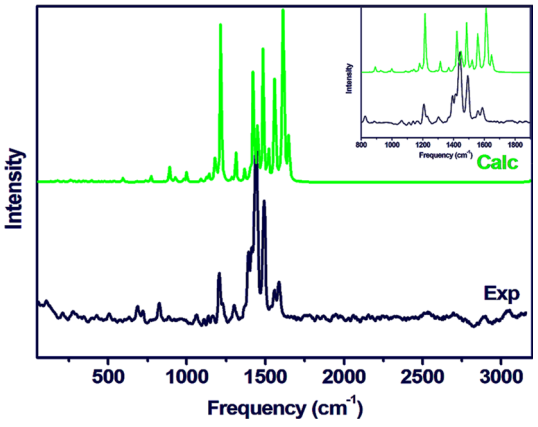

Fig. 7 Calculated and experimental Raman spectra of the Ni(II)-complex in the whole range (50–3200 cm^{-1}). Zoom view in the range of 800–1900 cm^{-1} (*inset*)

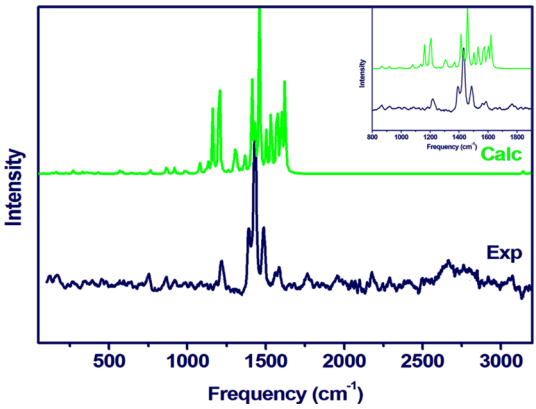

Fig. 8 Calculated and experimental Raman spectra of the [Cu(L)(H_2O)] complex in the whole range (50–3200 cm^{-1}). Zoom view in the range of 800–1900 cm^{-1} (*inset*)

Thermochemistry

The standard thermodynamic functions, namely, heat capacity ($C_{p,m}°$), entropy ($S_m°$) and enthalpy ($H_m°$) were calculated using the DFT/B3LYP method using the 6-31G basis set on the basis of harmonic vibrational analysis and statistical thermodynamics. The enthalpies, entropies, and heat capacities of both complexes calculated at different temperatures, in the range of 100–500 K and correlation equations are listed in Table 4. It is clear from Table 4 that the thermodynamic functions increase with increasing temperature. This may be due to increasing intensities of molecular vibration. The values of entropy ($S_m°$) and enthalpy ($H_m°$) were greater for the Cu(II)-complex compared to the Ni(II)-complex and vice versa for heat capacity ($C_{p,m}°$) values [15].

Non-linear optical properties

The quantum chemistry-based prediction of nonlinear optical (NLO) properties of a molecule has gained much attention in communication technology, optical switches, optical memory devices, etc. The total static dipole moment (μ), the linear polarizability (α), the anisotropy of the polarizability ($\Delta\alpha$), and the first hyperpolarizability (β) using the x, y, z components were calculated using the following equations [16, 28]:

$$\mu = \sqrt{\mu_x^2 + \mu_y^2 + \mu_z^2}, \tag{1}$$

$$\alpha = \frac{\alpha_{xx} + \alpha_{yy} + \alpha_{zz}}{3}, \tag{2}$$

$$\Delta\alpha = \frac{1}{\sqrt{2}} \sqrt{\left[\left(\alpha_{xx} - \alpha_{yy}\right)^2 + \left(\alpha_{yy} - \alpha_{zz}\right)^2 + \left(\alpha_{zz} - \alpha_{xx}\right)^2 + 6\alpha_{xx}^2 \right]} \tag{3}$$

Table 4 Thermodynamic properties of Ni(II)- and Cu(II)-complexes at different temperatures up to 500 K

T (K)	H_m° (kcal mol^{-1})		S_m° (cal mol^{-1} K^{-1})		$C_{p,m}^\circ$ (cal mol^{-1} K^{-1})	
	[Ni-L]	[Cu-L]	[Ni-L]	[Cu-L]	[Ni-L]	[Cu-L]
100	119.394	117.685	30.975	32.105	92.001	94.488
200	123.705	122.125	54.53	55.829	122.322	125.694
298.15	130.032	128.572	73.826	74.969	148.598	152.46
400	138.421	137.071	90.317	91.342	173.269	177.449
500	148.122	146.869	103.169	104.093	195.304	199.702

$H_m^\circ{}_{(Ni)} = 116.5976 + 0.01828T + 8.9826 \times 10^{-5}T^2$; $R^2 = 0.99991$

$H_m^\circ{}_{(Cu)} = 114.7456 + 0.0198T + 8.9267 \times 10^{-5}T^2$; $R^2 = 0.99991$

$S_m^\circ{}_{(Ni)} = 4.1381 + 0.2868T - 1.7771 \times 10^{-4}T^2$; $R^2 = 0.99999$

$S_m^\circ{}_{(Cu)} = 5.1979 + 0.2883T - 1.8127 \times 10^{-4}T^2$; $R^2 = 0.99997$

$C_{p,m}^\circ{}_{(Ni)} = 59.5626 + 0.3395T - 1.3665 \times 10^{-4}T^2$; $R^2 = 0.99997$

$C_{p,m}^\circ{}_{(Cu)} = 61.0734 + 0.3507T - 1.4753 \times 10^{-4}T^2$; $R^2 = 0.99996$

$$\beta = \sqrt{\left(\beta_{xxx} + \beta_{xyy} + \beta_{xzz}\right)^2 + \left(\beta_{yyy} + \beta_{xxy} + \beta_{yzz}\right)^2 + \left(\beta_{zzz} + \beta_{xxz} + \beta_{yyz}\right)^2}. \quad (4)$$

The dipole moment (μ), the linear polarizability (α), the anisotropy of the polarizability ($\Delta\alpha$), and the first hyperpolarizability (β) were calculated at the B3LYP/6-31G level. The calculated dipole moment (μ) for the Ni(II)- and the Cu(II)-complex were 2.9807 and 3.0473 D, respectively. The calculated linear polarizability (α) and the anisotropy of the polarizability ($\Delta\alpha$) were 157.411 and 290.5344 Å^3 respectively, for the Ni(II)-complex; 158.037 and 294.370 Å^3 respectively, for Cu(II)-complex. The first hyperpolarizability (β) was calculated for the Ni(II)- and Cu(II)-complex 2.6376×10^{-30} cm^5 esu^{-1} and 2.7890×10^{-30} cm^5 esu^{-1}, respectively.

Urea is one of the reference materials and frequently used for comparative purposes in the study of the NLO properties. The calculated values of μ, α, and β for those complexes were higher than those of urea (the μ, α, and β of urea are 1.3732 D, 3.8312 Å^3 and 0.37289×10^{-30} cm^5 esu^{-1} obtained by the B3LYP/6-31G method). Theoretically, the first-order hyperpolarizability (β) of both complexes was found to be about seven times higher than urea. These results indicate that both complexes may possess good non-linear optical properties.

Conclusion

Interaction of the 2,4-dichloro-6-{[(5-chloro-2-sulfanylphenyl)imino]methyl}phenol ligand with Ni(II) and Cu(II) metal ions in a tridentate mode resulted in the formation of two new mononuclear complexes. The thermogravimetric analysis of

the resulting Schiff base-metal complexes revealed their thermal stability. Thermal degradation of such complexes follows a first order kinetic model. The best results were obtained by the Coats–Redfern (C–R) method for evaluating non-isothermal kinetic parameters viz. E^*, Z, ΔS^*, ΔH^*, and ΔG^*. The thermal degradation process follows the random nucleation mechanism. The experimental FTIR and Raman spectra were compared with theoretical frequencies calculated at the B3LYP level using the 6-31G basis set and found to have appreciable results. The computed thermodynamic properties ($C_{p,m}^\circ$; S_m° and H_m°) show a polynomial relationship with increasing temperatures up to 500 K. The first-order hyperpolarizabilities were computed at the same level of theory for both complexes and results indicate that they may possess good nonlinear optical properties.

Acknowledgments We are thankful to the Head, Department of Chemistry, Dr. H. S. Gour Central University, Sagar India, for providing departmental facilities. We thank the Sophisticated Instrumentation Center, Dr. H. S. Gour Central University, Sagar for making available thermal analysis. We acknowledge the Sophisticated Analytical Instrument Facility (SAIF), Panjab University, Chandigarh, India for elemental analysis.

References

1. M.E. Brown, D. Dollimore, A.K. Galwey, *Comprehensive Chemical Kinetics* (Elsevier, Amsterdam, 1980)
2. M.E. Brown, *Techniques and Applications*, 2nd edn. (Kluwer, London, 2001)
3. S. Vyazovkin, Anal. Chem. **80**, 4301–4316 (2008)
4. A. Khawam, D.R. Flanagan, J. Pharm. Sci. **95**(3), 472–498 (2006)
5. J.A. Conesa, A. Marcilla, J.A. Caballero, R. Font, J. Anal. Appl. Pyrol. **58**(59), 617–633 (2001)
6. T. Sun, Y. Zhao, J. Jin, D. Wang, J. Therm. Anal. **45**, 1105–1109 (1995)
7. Q.P. Hu, X.G. Cui, Z.H. Yang, J. Therm. Anal. **48**, 1379–1384 (1997)
8. A.W. Coats, J.P. Redfern, Nature **201**, 68–69 (1964)
9. G.O. Piloyan, O.S. Novikova, Russ. J. Inorg. Chem. **12**, 313 (1966)
10. H.H. Horowitz, G. Metzger, Anal. Chem. **35**, 1464–1468 (1963)
11. S. Vyazovkin, C.A. Wight, Thermochim. Acta **340**(341), 53–68 (1999)
12. B.S. Kusmariya, A. Tiwari, A.P. Mishra, G.A. Naikoo, J. Mol. Struct. **1119**, 115–123 (2016). doi:10.1016/j.molstruc.2016.04.056
13. A. Bhunia, S. Manna, S. Mistri, A. Paul, R.K. Manne, M.K. Santra, V. Bertolasi, S.C. Mann, RSC Adv. (2015). doi:10.1039/C5RA12324K
14. R.C. Dunbara, J.D. Steill, J. Oomens, Int. J. Mass Spectrom. **297**, 107–115 (2010). doi:10.1016/j.ijms.2010.07.001
15. M. Odabasoglu, C. Albayrak, B. Kosar, O. Büyükgüngör, Spectrochim. Acta A **92**, 357–364 (2012). doi:10.1016/j.saa.2012.02.101
16. B.S. Kusmariya, A.P. Mishra, J. Mol. Struct. **1101**, 176–188 (2015). doi:10.1016/j.molstruc.2015.08.026
17. B.S. Kusmariya, A.P. Mishra, J. Mol. Model. **21**(278), 1–14 (2015). doi:10.1007/s00894-015-2805-z
18. M.A.D. Becke, Phys. Rev. A **38**, 3098 (1988)
19. C. Lee, W. Yang, R.G. Parr, Phys. Rev. B **37**, 785 (1988)
20. M.J. Frisch, G.W. Trucks, H.B. Schlegel, G.E. Scuseria, M.A. Robb, J.R. Cheeseman, J.A. Montgomery Jr., T. Vreven, K.N. Kudin, J.C. Burant, J.M. Millam, S.S. Iyengar, J. Tomasi, V. Barone, B. Mennucci, M. Cossi, G. Scalmani, N. Rega, G.A. Petersson, H. Nakatsuji, M. Hada, M. Ehara, K. Toyota, R. Fukuda, J. Hasegawa, M. Ishida, T. Nakajima, Y. Honda, O. Kitao, H. Nakai, M. Klene, X. Li, J.E. Knox, H.P. Hratchian, J.B. Cross, V. Bakken, C. Adamo, J. Jaramillo, R. Gomperts, R.E. Stratmann, O. Yazyev, A.J. Austin, R. Cammi, C. Pomelli, J.W. Ochterski, P.Y. Ayala, K. Morokuma, G.A. Voth, P. Salvador, J.J. Dannenberg, V.G. Zakrzewski, S. Dapprich, A.D. Daniels, M.C. Strain, O. Farkas, D.K. Malick, A.D. Rabuck, K. Raghavachari, J.B. Foresman, J.V. Ortiz, Q. Cui,

A.G. Baboul, S. Clifford, J. Cioslowski, B.B. Stefanov, G. Liu, A. Liashenko, P. Piskorz, I. Komaromi, R.L. Martin, D.J. Fox, T. Keith, M.A. Al-Laham, C.Y. Peng, A. Nanayakkara, M. Challacombe, P.M.W. Gill, B. Johnson, W. Chen, M.W. Wong, C. Gonzalez, J.A. Pople, *Gaussian 03, Revision D.01* (Gaussian Inc., Wallingford, 2004)
21. G.A. Zhurko; Chemcraft version 1.7(build375). http://www.chemcraftprog.com
22. R.K. Jain, A.P. Mishra, P. Gupta, J. Therm. Anal. Calorim. **110**, 529–534 (2012). doi:10.1007/s10973-012-2401-8
23. A. Khawam, D.R. Flanagan, J. Phys. Chem. B **110**(35), 17315–17328 (2006). doi:10.1021/jp062746a
24. S. Shukla, A.P. Mishra, J. Therm. Anal. Calorim. **107**, 111–117 (2012). doi:10.1007/s10973-011-1616-4
25. B.S. Kusmariya, S. Tiwari, A. Tiwari, A.P. Mishra, G.A. Naikoo, U.J. Pandit, J. Mol. Struct. **1116**, 279–291 (2016). doi:10.1016/j.molstruc.2016.03.029
26. F. Dogan, M. Ulusoy, O.F. Ozturk, I. Kaya, B. Saith, J. Therm. Anal. Calorim. **96**, 267–276 (2009)
27. N.T. Madhu, P.K. Radhakrishnan, W. Linert, J. Therm. Anal. Calorim. **84**, 607–611 (2006)
28. B. Kosar, C. Albayrak, Spectrochim. Acta A **78**, 160–167 (2011). doi:10.1016/j.saa.2010.09.016